Proceedings of Computational Engineering Conference JSCES
Vol. 28, 2023 May

A Liquid Film Simulation Using AMR-PLIC-HF method with Surfactant Transport

Tongda Lian [1] Shintaro Matsushita [2] and Takayuki Aoki [3]

[1] Doctoral student, Student of Tokyo Institute of Technology (2–12–1 Ookayama, Meguro-ku Tokyo 152–8550, E-mail: lian@sim.gsic.titech.ac.jp)
[2] Ph.D., Assistant Professor of Tokyo Institute of Technology (2–12–1 Ookayama, Meguro-ku Tokyo 152–8550, E-mail: matsushita.s.ad@m.titech.ac.jp)
[3] Ph.D., Professor of Global Science Information Center of Tokyo Institute of Technology (2–12–1 Ookayama, Meguro-ku Tokyo 152–8550, E-mail: taoki@gsic.titech.ac.jp)

In this study, the Piecewise Linear Interface Calculation (PLIC) method and Height Function (HF) method are implemented on adaptively refined mesh grids based on Adaptive Mesh Refinement (AMR) method. With the AMR method, the required computational resources can be greatly cut down without compromising the mass conservation or the accuracy. With the parallel computing techniques based on CUDA programming language and NVIDIA V100 GPU, the efficiency of simulation is improved. The Weakly Compressible Scheme (WCS) and pressure projection method is used in fluid analysis and improves the numerical stability. The Langmuir model is adopted in surfactant transport computations. The AMR-PLIC-HF method is verified by a time-reversed advection of a circle in a single vortex flow. The two-phase flow computation is verified by single bubble rising simulations with two sets of physical properties. The process of generation and rupture of a thin liquid film by a bubble freely rising to in liquid-gas interface is simulated with considering the surfactant transport and Marangoni Effect.

Key Words : *Liquid film, Surfactant, Langmuir model, PLIC-VOF, Height function Weakly compressible scheme, Tree-based AMR method, GPU computing*

1. INTRODUCTION

The interactions involving bubbles and droplets are ubiquitous in naturally occurring processes and in industrial processes and products. When bubbles or droplets collide or approach each other, liquid films are formed. The draining dynamics and stability of liquid films have been investigated by using theoretical models due to their importance to gas or droplet emulsion systems. With the development of numerical simulation of fluids, nowadays a wide range of fluid phenomena can be simulated. However, for the problems including liquid films, there have been only limited attempts to investigate by numerical simulations. The obstacles to application of numerical simulations to liquid film simulations are concluded into three aspects — multi-scale, interface capturing and fluid analysis.

In the thin liquid film simulation, the typical length is much larger than the thickness of thin liquid film. The typical length could be in milimeter, centimeter or even meter scales, while the thickness of thin liquid film is typically in the micrometer scale. To accurately describe the motion of the liquid film and its interfaces, the resolution of mesh grids needs to be extremely high, which makes it almost possible for limited computation resources—memory and execution time.

To overcome this obstacle, a tree-based AMR method is utilized in the present research [1]. To implement the AMR method on GPU, an extended stencil computation is proposed based on previous research [2]. The finest mesh grids are always resigned in the area that is close to the interfaces, which ensures the high-resolution mesh grids used to capture the interfaces of liquid films. For the region far away from the interfaces, the computational cells are coarsened to save computational resources while not compromising the accuracy of the interface computations.

The thin liquid films typically consist of two interfaces between different phases that are close to each other. Thus, the high-accuracy interface capturing method is essential to simulate thin liquid films. In previous research, the coupled Phase Field–Level Set method is found capable to capture the interfaces while maintaining the mass conservation and has satisfactory accuracy in geometric computations such as normal vector of interfaces. However, as a diffuse interface model, the Phase Field method could bring numerical error to simulations when the thickness of the diffuse interface is close to the thickness of the liquid film.

Since the Piecewise Linear Interface Calculation–Volume of Fluid (PLIC-VOF) method has a sharp interface model and is capable to suppress the spurious current, the PLIC-HF method is implemented on AMR mesh grids by GPU parallel computing techniques. With the second-order Mixed Youngs-Centered method, the normal vectors

of interfaces can be accurately obtained for VOF advection computations.

For the fluid analysis, the conventional solvers with implicit pressure Poisson equation is not suitable for parallel computing and has numerical stability issues when the density ratio of the heavy and light phases is extremely high. For water and air system, the density ratio is 830 times. Thus, the Weakly Compressible Scheme (WCS) and pressure projection method is used in fluid analysis [3]. With WCS and pressure projection method, even though the time step needs to be kept small, the execellent performance of GPU parallel computing overrides the defect and greatly improves the overall efficiency.

The Marangoni effect caused by temperature difference and gradient of surfactant concentration on interfaces is considered influence the stability and draining dynamics of thin liquid films. In the present work, the isothermal condition is assumed so only the concentration-induced Marangoni effect is considered. The Langmuir model is used to compute the adsorption and desorption of surfactant on the interfaces.

The purpose of the present work is to realize the direct numerical simulation of thin liquid films with surfactant transport with high efficiency and obtain high-accuracy results by using the proposed AMR-PLIC-HF method and GPU parallel computing.

2. NUMERICAL METHODS

(1) Governing Equations

The momentum equation in weakly compressible flow can be expressed by

$$\frac{\partial \boldsymbol{u}}{\partial t} + (\boldsymbol{u}\cdot\nabla)\,\boldsymbol{u} = -\frac{1}{\rho}\nabla p + \frac{1}{\rho}\nabla\cdot\boldsymbol{\tau} + \frac{1}{\rho}\boldsymbol{F}. \quad (1)$$

Since the present model assumes isothermal state and low Mach number condition, the evolution of pressure can be derived as

$$\frac{\partial p}{\partial t} = -\rho c_s^2 \nabla\cdot\boldsymbol{u}. \quad (2)$$

In **Eq.** (1) and **Eq.** (2), $\boldsymbol{u}$ is velocity, p is pressure, ρ is density, τ is viscous stress term and $\boldsymbol{F}$ is external force term. The external force $\boldsymbol{F}$ in the present work consists of gravity $\boldsymbol{F}_g$ and surface tension $\boldsymbol{F}_{sf}$. The surface tension $\boldsymbol{F}_{sf}$ is evaluated by a density-scaled Continuous Surface Force (CSF) model proposed by Yokoi[4].

The density is computed from the volume of fluid. The advection term in **Eq.** (1) is discretized by third order WENO scheme and other terms are discretized by second order central difference. Third order Runge-Kutta method is adopted for time integration. Staggered grid is used to avoid the decoupling of velocity and pressure and provide a better numerical stability by defining scalars on cell centers and vectors on cell faces.

(2) Interface Capturing by PLIC-VOF method

While the Phase Field method—as a diffuse interface capturing method—solves the Allen-Cahn equation or the Cahn-Hilliard equation with the consideration of diffusion and negative diffusion terms and keeps a certain width of the interface, the PLIC-VOF method linearizes the interfaces in each cell and regards them as a line in 2D space and a plain surface in 3D space.

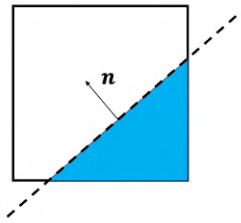

Fig. 1 Interface reconstruction in the Piecewise Linear Interface Construction (PLIC) method.

In the present study, simulations are performed in 2D space. Thus in each cell, the interface is considered as a line as shown in **Fig. 1** expressed by

$$\boldsymbol{n}\cdot\boldsymbol{x} = \alpha \quad (3)$$

where $\boldsymbol{n}$ indicates the normal vector of this linearized interface, $\boldsymbol{x}$ is the spacial coordinate and α is a constant to specify the position of the line.

The VOF function ϕ is advected by

$$\frac{\partial \phi}{\partial t}\Delta\Omega + F_{net} = \oint_\Omega c\nabla\cdot\boldsymbol{u}\,\mathrm{d}v \quad (4)$$

where $\Delta\Omega \equiv \int_\Omega 1\mathrm{d}v$ is defined as the volume of the cell. In **Eq.** (4), the value of the right-hand side should be zero because it is a divergence-free velocity field where $\nabla\cdot\boldsymbol{u}$ is zero. However, a dimensional split method [5] was used in the current research, which means that the flux calculation and time integration proceeded alternately i n the X-direction and Y-direction. One-direction velocity is not divergence-free; thus, the right-hand side could not be simply ignored. To conserve the volume, a simplification was adopted:

$$\oint_\Omega c\nabla\cdot\boldsymbol{u}\,\mathrm{d}v = c_c\frac{\partial u_d}{\partial x_d}\Delta\Omega \quad (5)$$

where d is the Cartesian index indicating the X-direction or Y-direction, and c_c is the value of the color function at the center of the cell and is defined explicitly as

$$c_c = \begin{cases} 1 & \text{if} \quad \phi > 1/2 \\ 0 & \text{else} \end{cases} \quad (6)$$

The density and viscosity of liquid-gas two-phase flow is computed by using VOF function by the equations shown below. The subscript l and g indicates the properties of heavy phase and light phase respectively.

$$\rho = \phi\rho_h + (1-\phi)\rho_l \quad (7)$$

$$\mu = \phi\mu_h + (1-\phi)\mu_l \quad (8)$$

The interface curvature can be calculated with an improved Height Function (HF) method [6] as expressed by

$$\kappa = \frac{H_{xx} + H_{yy} + H_{xx}H_y^2 + H_{yy}H_x^2 - 2H_{xy}H_xH_y}{\left(1 + H_x^2 + H_y^2\right)^{3/2}}. \tag{9}$$

where κ is the interface curvature, H is the height function calculated by volume fractions on a 3×7 or 7×3 stencil, and the subscripts x and y show the partial derivatives of the height function H. This method has a high level of accuracy even when the local grid resolution is low because a local monotonicity correction is included.

(3) Surfactant Transport Equation Considering Adsorption and Desorption of the Interface

The transportation, adsorption and desorption of surfactant are expressed by Langmuir model as:

$$\frac{\partial F}{\partial t} + \boldsymbol{u} \cdot \nabla F = D_F \nabla^2 F + j\delta(\psi). \tag{10}$$

$$\frac{Df}{Dt} - \boldsymbol{u} \cdot \nabla_s f(\boldsymbol{u} \cdot \boldsymbol{n}) \left(\nabla_s \cdot \boldsymbol{n}\right) = -\nabla_s \cdot (f\boldsymbol{u}) + D_f \nabla_f^2 f + j. \tag{11}$$

$$j = k_{\mathrm{ad}} F \left(f_{\mathrm{lim}} - f\right) - k_{\mathrm{de}} f. \tag{12}$$

where F is bulk concentration, f is interface concentration, j is the source term that express the adsorption and desorption between the bulk surfactant and the interface surfactant. k_{ad} and k_{de} are the adsorption and desorption rate coefficient correspondingly and f_{lim} is the saturation concentration. In the equations above, $\nabla_s = (\boldsymbol{I} - \boldsymbol{n} \otimes \boldsymbol{n})\nabla$ represents the gradient on the surface.

(4) Marangoni Effect Caused by Concentration Difference

The Marangoni effect is the free surface movement or flow along the interface that occurs due to the gradient in surface tension caused by the difference of temperature or surfactant concentration. In the present work, the simulations are in isothermal state. Therefore, the Marangoni effect due to the temperature difference is not considered, only the Marangoni effect due to the difference in the concentration of the surfactant is considered. The surfactant can lower the surface tension by being adsorbed to the interface. The change in surface tension coefficient depending on the concentration of the surfactant is well expressed by the following Marangoni state equation:

$$\sigma(f) = \sigma_0 \left[1 + \frac{RTf_{\mathrm{lim}}}{\sigma_0} \ln\left(1 - \frac{f}{f_{\mathrm{lim}}}\right)\right]. \tag{13}$$

Here, R is the gas constant of the ideal gas, T is the absolute temperature, and σ_0 is the surface tension coefficient when the surfactant concentration is 0. As shown in **Fig.2**, since **Eq.** (13) is a non-linear equation including logarithms, when the interface concentration f approaches f_{lim}, the surface tension coefficient asymptotically approaches $-\infty$, resulting in a very steep gradient.

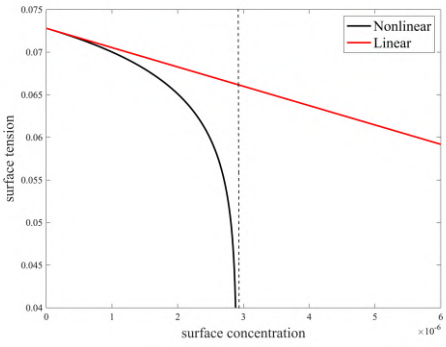

Fig. 2 Dependence of surface tension on interface concentration expressed by Langmuir model.

Linearized equation could improve the numerical stability but when the concentration f is near f_{lim}, the result has error shown in **Fig.2**. In present work, the following equation is used to set an upper limit for the concentration to prevent numerical instability:

$$\sigma(f) = \sigma_0 \left[1 + \frac{RTf_{\mathrm{lim}}}{\sigma_0} \ln\left(1 - \frac{\min(f, kf)}{f_{\mathrm{lim}}}\right)\right]. \tag{14}$$

Here, k is an adjustable parameter and is set as 0.95 in the present work.

The surface tension coefficient σ in conventional methods is considered as a constant value, but in the present research, σ becomes a function of f. The Marangoni effect due to the surface tension gradient in the tangential direction of the interface is expressed by the following equation.

$$\boldsymbol{F}_{\mathrm{sf}} = \sigma(f)\kappa + \nabla_s \sigma(f)\delta_\Gamma. \tag{15}$$

Here, $\nabla_s = (\boldsymbol{I} - \boldsymbol{n} \otimes \boldsymbol{n})\nabla$ represents taking the gradient on the surface. δ_Γ is a approximated delta function that takes positive value only near the interface. δ_Γ is defined as follows:

$$\delta_\Gamma \approx \frac{2}{dx}\phi^2(1 - \phi)^2. \tag{16}$$

where dx indicates the size of the finest computational cell.

3. TREE-BASED AMR AND IMPLEMENTATION

Simulating a multi-scale problem by using a uniform mesh grid is considered inefficient. For the region that is far away from the interface, it is not necessary to assign high-resolution mesh grids.

Thus, an improved Tree-based AMR method [7] is proposed and adopted in the present study. Fluid calculations are actually performed for the computational domain after subdivision, and in the tree structure, the terminal The terminal nodes and the block-shaped computational regions corresponding to these nodes are called leaves. To avoid complex implementation between leaves at different levels and to ensure numerical stability, the level difference between two adjacent leaves cannot be greater than one, which is called the 2:1 balance.

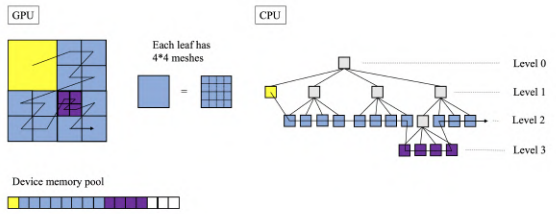

Fig. 3 Tree based AMR on GPU and CPU with space-filling curve.

As shown in **Fig. 3**, the tree data structure that manages the AMR structure is held only on the CPU side, and the leaves are arranged in a one-dimensional array on the GPU side. This information is stored as separate array data in a one-dimensional array arranged in the same order. Data that are candidates for refinement or coarsening are interpolated in parallel on the GPU.

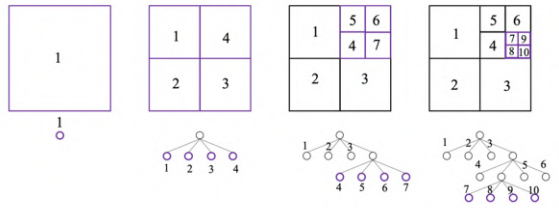

Fig. 4 The refinement procedure of tree based AMR.

As shown in **Fig. 4**, when a leaf node is subdivided by halving the grid width on each side, it is divided into four equal parts corresponding to the generation of 4 child nodes in 2D from the parent node. The refinement is performed recursively based on certain criteria

$$\min\left(|\psi_m|\right) < \sqrt{2} \times dh_{n+1} \times b. \tag{17}$$

where m represents the ID of the leaf, n represents the depth of the leaf m, and b is the number of cells in one direction in one leaf node. In the present research, the value of b was 4. According to **Eq.** (17), simply speaking, the current leaf node will be refined if the minimum distance to the interface in a leaf node is less than the diagonal block length of its child node.

In the present research, the reconstruction of the interface with the MYC scheme requires a 3×3 stencil that includes neighbor cells in diagonal directions. The HF method requires an even larger 3×7 or 7×3 stencil. The previous 8×8 stencil without a diagonal halo region is not sufficient for such computations. Thus, we propose an extended 12×12 stencil with a diagonal halo region to satisfy the stencil requirements of the MYC scheme and the HF method, as shown in **Fig. 5**. For the halo region in each direction, a 4×4 dataset is accessed and copied from the corresponding neighbor leaf. The diagonal neighbor leaves

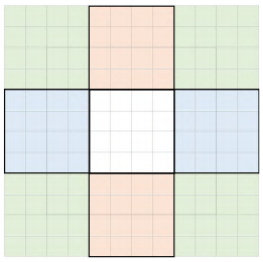

Fig. 5 The 12×12 stencil used in the present study.

shown in light green are accessed in a 'neighbor of neighbor' way. Since the MYC scheme and HF method are only used near to the interface to calculate the interface's normal vector and curvature, the 12×12 stencil is only used in these two computations. Additionally, since the AMR grid is interface-adapted, most refined meshes gather near the interface where there is no level difference. Thus, there is only access to diagonal neighbor leaves when the level difference is 0. This helps to reduce the need for computational resources, so the performance is not greatly compromised.

4. SIMULATIONS AND RESULTS

(1) Two-Dimensional Time-Reversed VOF Advection in a Single Vortex

A two-dimensional single vortex interface deformation simulation is performed, in which a vortex velocity field is designated in a fluid, and the interface between two phases is tracked as the vortex deforms the interface.

The size of the computational domain is $[0, 1] \times [0, 1]$. A circular interface with a radius of 0.2 is set at the initial position $(0.5, 0.75)$, and advection is performed according to the velocity field expressed by the following equations:

$$u(x, y, t) = 2\sin^2(\pi x)\sin(\pi y)\cos(\pi y)\cos\left(\frac{\pi t}{T}\right) \tag{18}$$

$$v(x, y, t) = -2\sin(\pi x)\cos(\pi x)\sin^2(\pi y)\cos\left(\frac{\pi t}{T}\right) \tag{19}$$

where, T is the period, which was set as 8.0 in the present research.

The interface is stretched by the flow field until $t = \frac{T}{2}$, and from $t = \frac{T}{2}$, the reverted velocity field is restored to its initial shape at $t = T$. In this calculation, $T = 8.0$ and the time step is set in accordance with the finest mesh size $\Delta t = 0.1\Delta x$.

An interface-adapted AMR method was used. The fine mesh was gathered near the interface according to the distance to the interface. As shown in **Fig. 6**, the initial tree node was 16×16 in size, and there were 4 cells in one direction on a leaf node. Thus, the initial resolution was 64×64. The finest resolution can be set by the maximum AMR refinement level. Two maximum levels were set at 2 and 3 with the finest resolutions being 256×256 and 512×512, respectively.

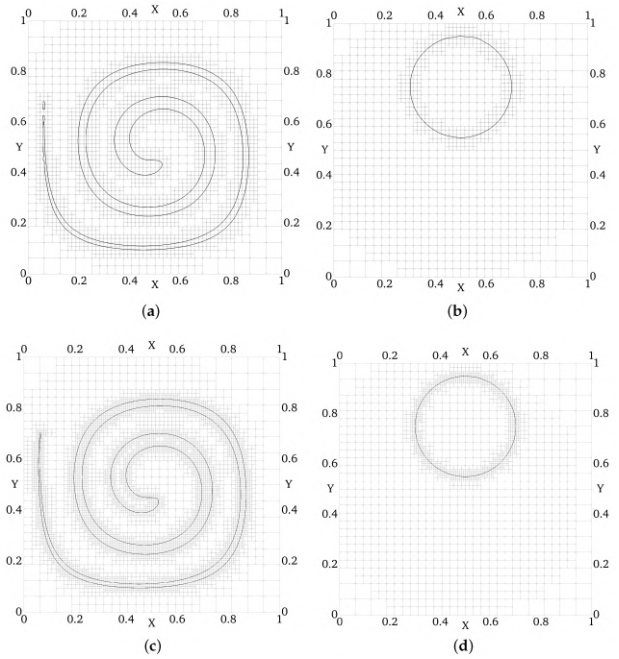

Fig. 6 Interface deformation in a 2D single vortex. (a) $t = \frac{T}{2}, 256 \times 256$**. (b)** $t = T, 256 \times 256$**. (c)** $t = \frac{T}{2}$**,** 512×512**. (d)** $t = T, 512 \times 512$**.**

Two-dimensional single rising bubble simulations [8] are performed to verify the accuracy of the proposed AMR-PLIC-HF method and the ability to solve two-phase flows as a benchmark test.

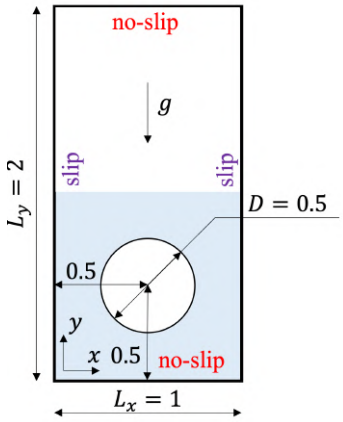

Fig. 7 A schematic diagram of liquid film generation and rupture simulation by a single bubble freely rising to an interface.

The configurations are shown in **Fig. 7**

Triton X-100[9] is used as the surfactant, the physical properties relevant to surfactant transportation is: $k_{ad} = 50.0[m^3/(mol \cdot s)]$, $k_{de} = 0.033[s^{-1}]$, $f_{lim} = 2.9 \times 10^{-6}[mol/m^3]$. The dimensionless Langmuir number to evaluate the the ease of desorption of the surfactant $La = F_0 k_{ad}/k_{de} = 15$. Therefore, the initial bulk concentration is $F_0 = 1.0 \times 10^{-2}[mol/m^3]$. The bubbles start rising from a contaminated state, which assumes that the interface and bulk concentration are in an equilibrium state, where $j = k_{ad}F(f_{lim} - f) - k_{de}f = 0$. Therefore, the initial interface concentration can be calculated out as $f_0 = 2.72 \times 10^{-6}[mol/m^3]$. For density, $\rho_h = 1000.0[kg/m^3]$, $\rho_l = 100.0[kg/m^3]$. For viscosity, $\mu_h = 10.0[Pa \cdot s]$, $\mu_l = 1.0[Pa \cdot s]$. The initial surface tension without decrease caused by Marangoni effect is $\sigma_0 = 24.5[kg/s^2]$. The gravity is set as $g = -0.98[m/s^2]$ in the $Y-$ direction.

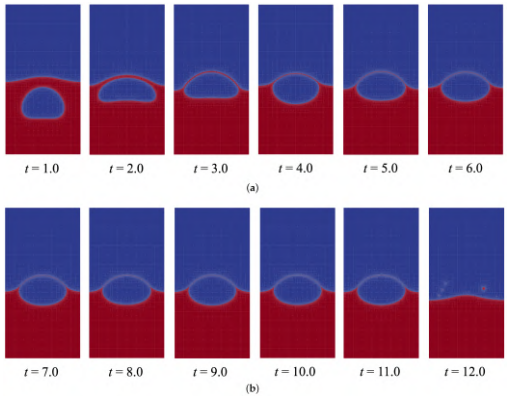

Fig. 8 Volume fraction profile for the bubble rising to an interface starting from the contaminated state and forming liquid film in surfactant solution with a Langmuir number of $La = 15$**, from** $t = 1.0$ **to** $t = 12.0$**.**

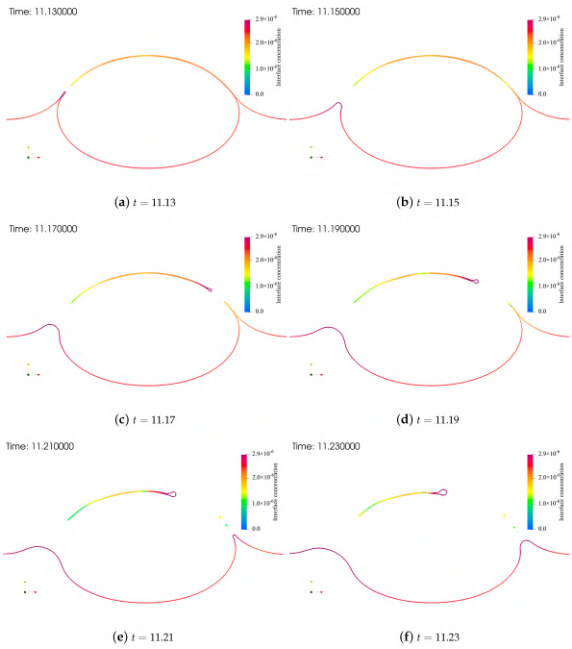

Fig. 9 Interface concentration profile focused on the liquid film area during the liquid film rupture process in surfactant solution with a Langmuir number of $La = 15$**.**

The volume fraction profile during the rising of the bubble and the generation of the liquid film is shown in **Fig. 8**. When the bubble started to rise, the bottom of the bubble became flat. At around $t = 2.0$, the upper part of the interface of the bubble approached the horizontal interface between the heavy fluid and light fluid. As the bubble continued to rise, the liquid layer over the bubble became thinner. After $t = 5.0$, with the drainage of the upper liquid layer, a thin liquid film was generated. The thin liquid film was kept stable until around $t = 11.0$. Since the present simulation used the PLIC-HF method, the influence of spurious current on the liquid film is greatly suppressed. Under the influence of gravity, drainage continued and the thickness of the thin liquid film gradually decreased. When the thickness of the thin liquid film reached a lower limit, rupture occurred on the liquid film at $t = 11.11$.

Fig. 9 shows the interface concentration p rofile during the liquid film rupture process from $t = 11.13$ to $t = 11.27$ with an interval of $\Delta t = 0.02$ when the Langmuir number was $La = 15$. It is observed that the upper rim on the left side has a later generation time. It is observed that, during the rupture process, the interface concentration is low at the point at which the rupture occurred, while the interface concentration is relatively high at the top of the interface concentration. This distribution can be explained by the motion of the liquid forming the liquid film. Due to the gradient of the interface concentration, the surface tension coefficient σ is low on the top and high on the left side.

5. CONCLUSION

In the present study, a AMR-PLIC-HF method is proposed and implemented by GPU parallel computing. The PLIC-HF method was applied to a tree-based interface-adaptive AMR mesh and used to simulate the generation and rupture of thin liquid film. It was used along with the WCS and the evolving pressure projection method as a fluid solver. The accuracy and efficiency of the solver were verified by benchmark tests including the single vortex flow. The processes of liquid film generation and rupture with surfactant transport and the Marangoni effect were directly simulated.

ACKNOWLEDGMENT :The authors would like to acknowledge the financial support received from the Grant-in-Aid for Scientific Research (S) 19H05613, Japan Society for the Promotion Science (JSPS), Joint/Research Center for Interdisciplinary Large-scale Information Infrastructures (JHPCN), jh200018 and jh210013, High Performance Computing Infrastructure (HPCI) hp210129 and hp230065 projects, and JST SPRING under grant number JPMJSP2106. The authors thank the Global Scientific Information and Computing Center, Tokyo Institute of Technology for the use of the TSUBAME 3.0 supercomputer and the Information Technology Center of Nagoya University for the use of the Flow Type II supercomputer. The authors would like to thank Kai Yang from the Tokyo Institute of Technology for his help with the programming and implementation of the PLIC-HF method.

REFERENCES

[1] Berger, M.J. and Oliger, J.: Adaptive mesh refinement for hyperbolic partial differential equations, J. Comput. Phys., Vol. 53, No.3, pp.484–512, 1984.

[2] Matsushita, S. and Aoki, T.: Gas-liquid two-phase flows simulation based on weakly compressible scheme with Interface-adapted AMR method, J. Comput. Phys., Vol.445, 110605, 2021.

[3] Yang, K. and Aoki. T.: Weakly compressible Navier-Stokes solver based on evolving pressure projection method for two-phase flow simulations, J. Comput. Phys., Vol.431, 110113, 2021.

[4] Yokoi, K.: A density-scaled continuum surface force model within a balanced forceformulation, J. Comput. Phys., Vol.278, pp.221–228, 2014.

[5] Weymouth, G. D. and Yue D.K.: Conservative Volume-of-Fluid Method for Free-surface Simulations on Cartesian-grids. J. Comput. Phys., 229(8):2853-2865, 2010.

[6] Lopez, J., Zanzi, C., Gomez, P., Zamora, R., Faura, F. and Hernandez, J.: An Improved Height Function Technique for Computing Interface Curvature from Volume Fractions. Comput Methods Appl. Mech. Eng., 198(33–36):2555-2564, 2009.

[7] Lian, T., Matsushita, S. and Aoki, T.: An AMR-Based Liquid Film Simulation with Surfactant Transport Using PLIC-HF Method, Appl. Sci. 2023, 13(3), 1955;

[8] Hysing, S., Turek, S., Kuzmin, D., Parolini, N., Burman, E., Ganesan, S. and Tobiska, L.: Quantitative Benchmark Computations of Two-dimensional Bubble Dynamics. Int. J. Numer. Methods Fluids 2009, 60, 1259-1288.

[9] Lin, S-Y. and Chang, H-C. and Chen, E-M.: The Effect of Bulk Concentration on Surfactant Adsorption Processes: The Shift from Diffusion-Control to Mixed Kinetic-Diffusion Control with Bulk Concentration, J. chem. eng. Jpn, Vol.29, pp.634–641, 1996.